Journal of Magnetism and Magnetic Materials 587 (2023) 171281

Contents lists available at ScienceDirect

Journal of Magnetism and Magnetic Materials

journal homepage: www.elsevier.com/locate/jmmm

Research article

Choosing the best magnetostrictive material for energy harvesting applications: A simple criterion based on Ericsson cycles

Laurent Daniel [a,b,*], Benjamin Ducharne [c,d], Yuanyuan Liu [c,d], Gael Sebald [d]

[a] Université Paris-Saclay, CentraleSupélec, CNRS, Laboratoire de Génie Electrique et Electronique de Paris, 91192, Gif-sur-Yvette, France
[b] Sorbonne Université, CNRS, Laboratoire de Génie Electrique et Electronique de Paris, 75252, Paris, France
[c] Univ. Lyon, INSA Lyon, LGEF EA682, Villeurbanne, France
[d] ELyTMaX IRL3757, CNRS, Univ Lyon, INSA Lyon, Centrale Lyon, Université Claude Bernard Lyon 1, Tohoku University, Sendai, Japan

ARTICLE INFO

Keywords:
Energy harvesting
Magnetostriction
Ericsson cycle
Analytical criterion
Ultimate harvestable energy

ABSTRACT

The best magnetostrictive material for energy harvesting applications is not necessarily the material with the highest magnetostriction strain. In this paper, based on the description of the Ericsson cycle, a simple criterion to define the most efficient material is proposed. The criterion takes into account the accessible range of stress and magnetic field. It relies on four material parameters only, namely the initial magnetic susceptibility, the saturation magnetisation, the maximum magnetostriction strain and the coercive field of the considered magnetostrictive material. Mass density and price are also involved if a weight optimisation or a cost optimisation is sought. The potential of several materials is compared based on this approach, and it is shown that Giant Magnetostrictive Materials are not systematically the best choice for energy harvesting applications, challenged for some operating conditions by electrical steels.

1. Introduction

Energy harvesting (power harvesting or energy scavenging) is the process of capturing energy from a system's environment and converting it into usable electrical power [1]. One driving force behind the search for new energy-harvesting devices is the desire to power sensor networks and mobile devices without batteries requiring external charging or service. This statement is especially valid in the rapidly growing field of the Internet of Things (IoTs) [2,3]. Various energy sources, such as wind, solar, geothermal, hydropower, or vibration can be considered. All these methods have pros and cons, but the needs for alternative energy are so significant that none of them can really be left apart from scientific investigations.

This work focuses on vibration. It has many advantages, such as availability, energy levels in the range of IoTs needs, and ubiquity [4,5]. Here, energy is scavenged from ambient mechanical vibrations of multiple origins (vehicles, machinery, etc.) and physical characteristics (with frequencies from 0.1 Hz to 1 kHz and accelerations from 0.01 to 1 g) [6].

Due to the extensive range of vibration properties, various designs of harvesters have been described in the scientific literature [7–9]. Vibration energy harvesters can be classified as electromagnetic or electrostatic when no active conversion occurs. In that case, the vibration source induces a relative motion between coils and permanent magnets (electromagnetic [10]) or movable electrodes (electrostatic [11]). Oppositely, active energy harvesters use functional materials (mainly piezoelectric [12] or magnetostrictive [6]) that convert mechanical energy into a magnetic or electrical energy form. Piezoelectric materials show a high coupling coefficient but are brittle, can be depolarised, and exhibit high output impedances [6]. Regarding these aspects, magnetostrictive materials are much more adapted even if they also show limitations like their highly nonlinear behaviour [6].

Many energy-harvesting devices based on magnetostrictive materials have been proposed [6,13,14]. They have made use of various magnetic materials such as Terfenol-D [15–18], Galfenol [19–23], Iron-based amorphous alloys [7,24,25] or Iron–Cobalt alloys [26,27]. The choice of the material is usually made a priori, before the design of the energy harvesting device. However, comparing the performance of magnetostrictive materials in the energy harvesting context is mandatory for designing optimal harvesters.

It raises many questions:

- Is the best material necessarily the one with the highest magnetostriction coefficient?
- Are there any optimal loading conditions?

* Corresponding author at: Université Paris-Saclay, CentraleSupélec, CNRS, Laboratoire de Génie Electrique et Electronique de Paris, 91192, Gif-sur-Yvette, France.
E-mail address: laurent.daniel@centralesupelec.fr (L. Daniel).

https://doi.org/10.1016/j.jmmm.2023.171281
Received 6 July 2023; Received in revised form 23 August 2023; Accepted 18 September 2023
Available online 21 September 2023

∘ Is a bias magnetic field required to improve the conversion efficiency?

∘ What would be the ultimate amount of energy converted? And what are the parameters driving this value?

Multiple experimental results are available in the scientific literature, but the working conditions are always different, making such comparisons impossible. Alternatively, this study proposes a simple analytical expression to predict the level of magnetostrictive conversion and to answer these questions. The model constitutes a decision tool for a given loading condition regarding volume, weight, or price optimisation. 3D stress configurations are considered, and the approach requires only four material parameters, easily found in the literature: the magnetisation saturation M_s, the maximum magnetostriction strain λ_s, the maximum permeability χ^o and the coercive field H_c (replaced by an applied bias field H_b if relevant).

This study is intended to assess the energy conversion capability of magnetostrictive materials, therefore, no specific device or electrical interface will be considered. The investigation is restricted to the pure magneto-mechanical conversion. The design of magnetic circuits, coils, and associated instrumentation will not be discussed.

The paper is organised as follows: The thermodynamic Ericsson cycles used to assess the mechano-magnetic conversion are introduced first. The analytical model to define the proposed criterion is then described. A comparison between different materials available for energy harvesting applications is finally proposed, followed by a general conclusion.

2. The ericsson cycle as a mean to assess energy harvesting capabilities

Thermodynamic cycles are required to evaluate the converted energy appropriately [28]. In this work, we opt for the magnetostrictive Ericsson cycle as an image of energy conversion capability. The Ericsson cycle consists of two branches at constant mechanical stress and two others at constant magnetic field (see Fig. 1 for illustration and [28, 29] for additional explanations about Ericsson cycles). Considering a magnetostrictive specimen, the Ericsson cycle is covered in four steps shown in Fig. 1, starting from state 1 with no applied magnetic field ($\mathbf{H} = \mathbf{0}$) and a stress state $\boldsymbol{\sigma} = \boldsymbol{\sigma}_1$:

∘ Stage 1 to 2: the magnetic field $\mathbf{H}$ is kept at $\mathbf{0}$ and the stress $\boldsymbol{\sigma}$ is changed from $\boldsymbol{\sigma}_1$ to $\boldsymbol{\sigma}_2$.

∘ stage 2 to 3: the stress $\boldsymbol{\sigma}$ is kept at $\boldsymbol{\sigma}_2$ and the magnetic field $\mathbf{H}$ is changed from $\mathbf{0}$ to $\mathbf{H}_{\max}$.

∘ stage 3 to 4: the magnetic field $\mathbf{H}$ is kept at $\mathbf{H}_{\max}$ and the stress $\boldsymbol{\sigma}$ is changed from $\boldsymbol{\sigma}_2$ to $\boldsymbol{\sigma}_1$.

∘ stage 4 to 1: the stress $\boldsymbol{\sigma}$ is kept at $\boldsymbol{\sigma}_1$ and the magnetic field $\mathbf{H}$ is changed from $\mathbf{H}_{\max}$ back to $\mathbf{0}$.

The resulting loop area (grey zone in Fig. 1) in the $B(H)$ plane (where B is the magnetic flux density) can be considered an image of the ultimate magneto-elastic energy conversion capability of the material. In that sense, whatever the electrical interface, the converted energy will not be higher than the Ericsson cycle area. This area can therefore be considered an indicator of the conversion capability, and different materials can be compared accordingly. The approach is meant as a general assessment of the energy harvesting potential of magnetostrictive materials, but the possibility to use practically the Ericsson cycle as a mean of energy harvesting is discussed in Appendix.

3. Simplified calculation of the ericsson energy area

The purpose of this section is to provide an analytical expression for the Ericsson cycle area, based on an analytical definition of the anhysteretic magnetisation curve.

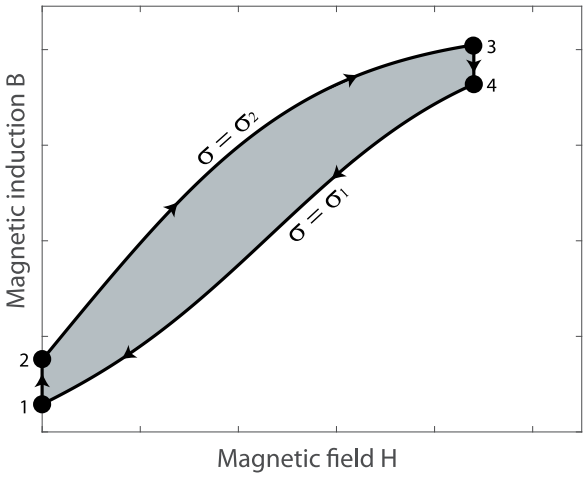

Fig. 1. Ericsson cycle.

3.1. Analytical definition of the magnetisation curve

The works in [30] provide an analytical expression for the stress-dependent anhysteretic magnetisation curve of ferromagnetic materials. The magnetisation $\mathbf{M}$ is expressed as:

$$\mathbf{M} = \frac{A_x \sinh(\kappa H)}{A_x \cosh(\kappa H) + A_y + A_z} M_s \mathbf{x}, \tag{1}$$

where H is the amplitude of the magnetic field $\mathbf{H}$ applied along direction $\mathbf{x}$ ($\mathbf{H} = H\,\mathbf{x}$). The coefficients A_x, A_y and A_y are functions of the applied stress $\boldsymbol{\sigma}$:

$$A_x = \exp(\alpha\,\sigma_{xx}); \quad A_y = \exp(\alpha\,\sigma_{yy}); \quad A_z = \exp(\alpha\,\sigma_{zz}) \tag{2}$$

where σ_{xx} (resp. σ_{yy}, σ_{zz}) is the principal component of the stress tensor $\boldsymbol{\sigma}$ along direction $\mathbf{x}$ (resp. $\mathbf{y}$, $\mathbf{z}$). The expression (1) introduces three material parameters M_s, κ and α. M_s is the saturation magnetisation of the material. It was shown in [30] that κ and α can be connected to standard material parameters according to (3).

$$\kappa = \frac{3\,\chi^o}{M_s} \quad \text{and} \quad \alpha = \frac{9\,\lambda_s\,\chi^o}{2\,\mu_0\,M_s} \tag{3}$$

χ^o is the initial (at no applied field) anhysteretic susceptibility of the material under stress-free conditions. It can reasonably be approximated by the maximum stress-free magnetic relative permeability of the material. λ_s is the maximum magnetostriction strain of the material, and μ_0 is the vacuum permeability.

Using these relations the anhysteretic stress-dependent magnetisation curve of a material can be defined using only three standard material parameters: the saturation magnetisation M_s, the maximum magnetostriction λ_s and the maximum magnetic susceptibility (or relative magnetic permeability) χ^o.

Due to the very strong assumptions made to obtain such a simple expression [30], the model cannot be expected to be as accurate as the full multiscale approaches from which it is derived [31–33], and it may struggle in some cases to describe quantitatively the magnetisation for a given magneto-elastic loading ($\mathbf{H}$, $\boldsymbol{\sigma}$). However the model was shown to predict the correct trends for the magneto-elastic behaviour (see for instance [30] for an application to an Iron–Cobalt alloy or [34] for an application to Terfenol-D). Moreover, in the following, the model will be integrated over large spans of magnetic field, which tends to compensate for local inaccuracies.

3.2. Analytical definition of the ericsson energy area

We now consider two anhysteretic magnetisation curves of a given material. A first curve under a stress state $\boldsymbol{\sigma}_1$, and a second curve under

a stress state $\boldsymbol{\sigma}_2$. The area $A_v(H_m, \boldsymbol{\sigma}_1, \boldsymbol{\sigma}_2)$ of the corresponding Ericsson cycle for a maximum field H_m is simply given by (4) in which we assume that $\boldsymbol{\sigma}_1$ and $\boldsymbol{\sigma}_2$ have been ordered so that $A_v(H_m, \boldsymbol{\sigma}_1, \boldsymbol{\sigma}_2) > 0$ (otherwise an absolute value can be added to (4)).

$$A_v(H_m, \boldsymbol{\sigma}_1, \boldsymbol{\sigma}_2) = \int_{H_b}^{H_b+H_m} \left(B(H_m, \boldsymbol{\sigma}_2) - B(H_m, \boldsymbol{\sigma}_1) \right) dH \tag{4}$$

H_b is a magnetic field, larger than the coercive field, that can be applied to consider a bias field and/or the hysteresis loss in the harvested energy calculus. In the case no bias-field is applied, the value of H_b is taken as the coercive field H_c. Using the expression of the stress-dependent anhysteretic magnetisation curve (1), the development of (4) yields the fully analytical expression (5) for the area of the Ericsson cycle in the general 3D-case.

$$\begin{aligned} A_v(H_m, \boldsymbol{\sigma}_1, \boldsymbol{\sigma}_2) = {} & \frac{\mu_0 M_s}{\kappa} \\ & \times \ln\left(\frac{A_x(\boldsymbol{\sigma}_2)\cosh(\kappa\,(H_b + H_m)) + A_y(\boldsymbol{\sigma}_2) + A_z(\boldsymbol{\sigma}_2)}{A_x(\boldsymbol{\sigma}_1)\cosh(\kappa\,(H_b + H_m)) + A_y(\boldsymbol{\sigma}_1) + A_z(\boldsymbol{\sigma}_1)} \right. \\ & \left. \times \frac{A_x(\boldsymbol{\sigma}_1)\cosh(\kappa\,H_b) + A_y(\boldsymbol{\sigma}_1) + A_z(\boldsymbol{\sigma}_1)}{A_x(\boldsymbol{\sigma}_2)\cosh(\kappa\,H_b) + A_y(\boldsymbol{\sigma}_2) + A_z(\boldsymbol{\sigma}_2)} \right) \end{aligned} \tag{5}$$

This expression gives the area of the Ericsson cycle in terms of Energy per volume unit. It can also be useful to describe the potential of a material in terms of energy per mass unit or in terms of energy per price unit. The corresponding expressions $A_m(H_m, \boldsymbol{\sigma}_1, \boldsymbol{\sigma}_2)$ and $A_\$(H_m, \boldsymbol{\sigma}_1, \boldsymbol{\sigma}_2)$ are given by (6), where ρ is the mass density of the material and $p_\$$ its price per mass unit.

$$\begin{aligned} A_m(H_m, \boldsymbol{\sigma}_1, \boldsymbol{\sigma}_2) &= \frac{1}{\rho} A_v(H_m, \boldsymbol{\sigma}_1, \boldsymbol{\sigma}_2) \quad \text{and} \\ A_\$(H_m, \boldsymbol{\sigma}_1, \boldsymbol{\sigma}_2) &= \frac{1}{p_\$} A_m(H_m, \boldsymbol{\sigma}_1, \boldsymbol{\sigma}_2) = \frac{1}{\rho\, p_\$} A_v(H_m, \boldsymbol{\sigma}_1, \boldsymbol{\sigma}_2) \end{aligned} \tag{6}$$

3.3. Simplification in the case of uniaxial stress applied along the field direction

In the case where one of the curves used for the Ericsson cycle is the stress-free magnetisation curve ($\boldsymbol{\sigma}_2 = \mathbf{0}$) and the second is a curve obtained under a uniaxial stress with amplitude σ applied parallel to the applied field ($\boldsymbol{\sigma}_1 = \sigma\, \mathbf{x} \otimes \mathbf{x}$), the area $A_v(H_m, \sigma, 0)$ of the Ericsson cycle simplified into (7). A positive (resp. negative) value of σ denotes a tensile (resp. compressive) stress.

$$A_v(H_m, \sigma, 0) = \frac{\mu_0 M_s}{\kappa} \ln\left(\frac{\exp(\alpha\,\sigma)\cosh(\kappa\, H_b) + 2}{\exp(\alpha\,\sigma)\cosh(\kappa\, H_m) + 2} \times \frac{\cosh(\kappa\, H_m) + 2}{\cosh(\kappa\, H_b) + 2} \right) \tag{7}$$

3.4. Ultimate achievable energy conversion under uniaxial stress

Assuming that it is possible to reach any level of magnetic field, it is interesting to see what is, for a given uniaxial stress σ, the ultimate area $A_v(H_\infty, \sigma, 0)$ that can be covered by the Ericsson cycle. The expression (8) is simply obtained by taking the limit of (7) when H_m tends to infinity.

$$A_v(H_\infty, \sigma, 0) = \frac{\mu_0 M_s}{\kappa} \ln\left(\frac{\cosh(\kappa\, H_b) + 2\, \exp(-\alpha\,\sigma)}{\cosh(\kappa\, H_b) + 2} \right) \tag{8}$$

4. Comparison of different materials for energy harvesting applications

This section is dedicated to the comparison of different materials regarding their potential for energy harvesting applications, based on their respective properties. The tested magnetic materials are listed in Table 1 with their relevant properties, taken from the literature. For the sake of simplicity, and although the proposed analytical approach can assess the potential of a material for any multiaxial loading, the analysis is here restricted to uniaxial loading configurations (uniaxial stress σ applied parallel to the magnetic field H).

4.1. Comparison based on volume efficiency

A first comparison can be made based on the maximum harvestable energy per volume unit. Based on (7), Table 2 shows the performance of the tested materials for various uniaxial stress σ (compressive) and various maximum field levels H_m. For each couple (H_m, σ), the better performance is indicated in dark colour and materials still competitive with the best performance are indicated in light colour.

At high levels of magnetic field H_m (of the order of 100 kA m^{-1}), Giant Magnetostrictive Materials (GMM, Terfenol-D and Galfenol), clearly show the best performance. If low levels of magnetic field H_m are considered, competitors emerge. FeNi and Fe-based amorphous alloys at low stress levels and GO FeSi or Polycrystalline Fe for higher stress levels reveal better capability than GMM in these ranges. This is due to the low magnetic permeability of GMM which requires high levels of applied magnetic field to exploit their full potential.

4.2. Comparison based on weight efficiency

Combining (7) with the left part of (6), the tested materials can be compared based on the maximum harvestable energy per mass unit. Given the small differences in the mass density between the tested materials, such a comparison brings essentially the same results as the comparison based on the maximum harvestable energy per volume unit. Therefore it will not be detailed here.

4.3. Comparison based on cost efficiency

Combining (7) with the right part of (6), a comparison based on price can be performed. It will reveal the maximum harvestable energy per price unit. The results are given in Table 3, showing under the same uniaxial loading conditions as Table 2. Again, for each couple (H_m, σ), the better performance is indicated in dark colour and materials still competitive with the best performance are indicated in light colour.

It is evident that the conclusions are very different compared to the case where volume (or weight) is to be optimised. Due to their very high price, GMM are not competitive anymore. Electrical steels on the contrary are produced in huge quantities, resulting in a very low cost, making them very competitive here for energy harvesting applications. Of course, these conclusions can evolve drastically based on price fluctuations, or required material quantity, but the proposed simple analytical formulas (7) and (6) allow for an updated view may price vary or other materials emerge.

4.4. Maximum harvestable energy for a given magneto-mechanical loading

Still considering uniaxial loadings, for the sake of simplicity, it is interesting to look, based on the available material database, at the best achievable harvested energy for a given stress σ and magnetic field H_m. Depending on the couple (H_m, σ), this best achievable harvested energy will be provided by different materials. The space (H_m, σ) for compressive stress has been scanned for all materials in Table 1, and the maximum harvestable energy has been picked up for all loading conditions. The results are shown in Fig. 2. Fig. 3 shows a performance map, to highlight which material is the most efficient, depending on the loading conditions and on the chosen criterion (volume or price).

High conversion performance, in terms of volume (and mass), can only be achieved by reaching very high field levels. Such configurations correspond to regions where GMM exhibit very high performance. On the contrary high conversion performance in terms of cost does not require very high levels of magnetic field. This is due to the competitiveness of electrical steels at low magnetic field H_m. It is interesting to note that Iron-Silicon steels dominate the competition if the cost is the chosen criterion (Fig. 3(b)). This is due to their price much lower than their competitors. This conclusion can change very quickly if the market conditions are changed. On the other hand, the landscape is very different if the criterion relies on volume efficiency (Fig. 3(a)). Depending on the loading conditions, very different materials can reveal as the most efficient in terms of energy harvesting.

Table 1
Choice of magnetostrictive candidates for energy harvesting applications: saturation magnetisation M_s, maximum magnetostriction λ_s, initial anhysteretic susceptibility of the stress-free magnetisation curve χ^o, coercive field H_c, mass density ρ, price $p_\$$.

	M_s 10^6 A m^{-1}	λ_s 10^{-6}	χ^o[a] –	H_c A m^{-1}	ρ kg m^{-3}	$p_\$$[b] \$ kg^{-1}	Ref.[c]
Polycrystalline Iron (Poly Fe)	1.72	5.0	50 000	10	7867	10	[35]
Non-oriented Iron Silicon steel (FeSi NO)	1.69	10	10 000	30	7700	1.2	[35]
Grain-oriented Iron Silicon steel (FeSi GO)	1.61	3.0	80 000	4	7650	1.5	[35]
Permalloy (FeNiMo)	0.64	1.0	500 000	1	8700	30	[35]
Permendur (FeCo-2V)	1.87	60	2000	30	8200	100	[35]
Fe50-Ni50	1.27	25	100 000	4	8120	40	[35]
Fe-based amorphous alloys (Fe-amorph)	1.24	40	100 000	2	7500	100	[35]
Co-based Amorphous alloys (Co-amorph)	0.49	0.5	500 000	1	7500	100	[35]
Nanocrystalline alloys (Finemet)	0.99	2.0	500 000	1	7200	14	[35]
Nanocrystalline alloys (Nanoperm)	1.21	0.1	50 000	3	7200	14	[35]
Terfenol-D	0.80	700	10	2500	9200[d]	15 000	[36]
Galfenol	1.38	200	20	150	7800[d]	10 000	[37]

[a] When not directly available, the maximum magnetic permeability was used.
[b] Prices can be subjected to considerable variations based on time and volume.
[c] Except for price, found at various suppliers online.
[d] Mass density for Terfenol-D and Galfenol were obtained from http://tdvib.com.

Table 2
Comparison based on volume efficiency: area $A_v(H_m, \sigma, 0)$ of the Ericsson cycle (in μJ cm^{-3}) for different materials under different loading conditions. Uniaxial stress is compressive ($\sigma < 0$). The cells coloured in dark colour highlight the best performance. A light colour indicates a competitive performance - though not first rank.

H_m (A m^{-1})	10^2	10^3	10^4	10^5	10^2	10^3	10^4	10^5	10^2	10^3	10^4	10^5	10^2	10^3	10^4	10^5
$\lvert\sigma\rvert$ (MPa)	10	10	10	10	25	25	25	25	50	50	50	50	100	100	100	100
Poly Fe	62	63	63	63	154	174	174	174	169	362	362	362	169	737	737	737
FeSi NO	31	114	114	114	52	324	324	324	56	696	696	696	56	1.4k	1.4k	1.4k
FeSi GO	39	39	39	39	106	106	106	106	176	219	219	219	177	444	444	444
Permalloy	15	15	15	15	37	37	37	37	75	75	75	75	79	150	150	150
Permendur	7	490	702	702	11	979	2.0k	2.0k	11	1.1k	4.2k	4.2k	11	1.1k	8.7k	8.7k
Fe50-Ni50	147	371	371	371	147	934	934	934	147	1.6k	1.9k	1.9k	147	1.6k	3.7k	3.7k
Fe-amorph	144	597	597	597	144	1.5k	1.5k	1.5k	144	1.5k	3.0k	3.0k	144	1.5k	1.5k	1.5k
Co-amorph	7	7	7	7	19	19	19	19	37	37	37	37	62	75	75	75
Finemet	30	30	30	30	75	75	75	75	123	150	150	150	123	300	300	300
Nanoperm	1	1	1	1	3	3	3	3	5	5	5	5	12	12	12	12
Terfenol-D	10	8	141	6.3k	21	17	308	16k	31	26	471	32k	38	32	571	50k
Galfenol	0	1	61	1.9k	0	2	150	4.7k	0	3	290	9.7k	0	5	533	20k

Table 3
Comparison based on cost efficiency: area $A_\$(H_m, \sigma, 0)$ of the Ericsson cycle (in μJ \$$^{-1}$) for different materials under different loading conditions. Uniaxial stress is compressive ($\sigma < 0$). The cells coloured in dark colour highlight the best performance. A light colour indicates a competitive performance - though not first rank.

H_m (A m^{-1})	10^2	10^3	10^4	10^5	10^2	10^3	10^4	10^5	10^2	10^3	10^4	10^5	10^2	10^3	10^4	10^5
$\lvert\sigma\rvert$ (MPa)	10	10	10	10	25	25	25	25	50	50	50	50	100	100	100	100
Poly Fe	792	796	796	796	2.0k	2.2k	2.2k	2.2k	2.1k	4.6k	4.6k	4.6k	2.1k	9.4k	9.4k	9.4k
FeSi NO	3.4k	12.3k	12.3k	12.3k	5.6k	35.1k	35.1k	35.1k	6.1k	75.3k	75.3k	75.3k	6.1k	156k	156k	156k
FeSi GO	3.4k	3.4k	3.4k	3.4k	9.2k	9.3k	9.3k	9.3k	15.4k	19.1k	19.1k	19.1k	15.4k	38.7k	38.7k	38.7k
Permalloy	56	56	56	56	142	142	142	142	286	286	286	286	303	573	573	573
Permendur	9	598	857	857	13	1.2k	2.4k	2.4k	14	1.4k	5.1k	5.1k	14	1.4k	10.6k	10.6k
Fe50-Ni50	452	1.1k	1.1k	1.1k	452	2.9k	2.9k	2.9k	452	4.9k	5.8k	5.8k	452	4.9k	11.5k	11.5k
Fe-amorph	192	796	796	796	192	2.0k	2.0k	2.0k	192	2.1k	4.0k	4.0k	192	2.1k	2.1k	2.1k
Co-amorph	10	10	10	10	25	25	25	25	50	50	50	50	82	100	100	100
Finemet	294	294	294	294	740	740	740	740	1.2k	1.5k	1.5k	1.5k	1.2k	3.0k	3.0k	3.0k
Nanoperm	10	10	10	10	25	25	25	25	53	53	53	53	114	114	114	114
Terfenol-D	<1	<1	1	46	<1	<1	2	119	<1	<1	3	233	<1	<1	4	362
Galfenol	<1	<1	1	24	<1	<1	2	61	<1	<1	4	125	<1	<1	7	258

4.5. Ultimate harvestable energy conversion

Another comparison that can be made between the different magnetostrictive materials consists in plotting the ultimate achievable energy conversion under uniaxial stress (compression). The results are shown in Fig. 4, for a comparison based on volume (left) and a comparison based on cost (right). It is reminded that a comparison based on the ultimate harvestable energy conversion supposes that the maximum level of magnetic field H_m required to obtained the best performance of a given material is attainable.

As expected, GMM show the best performance in terms of volume optimisation. In terms of cost optimisation, electrical steels are the best materials. Fig. 4 also shows that some materials are clearly not competitive for energy harvesting applications (e.g. Co-based amorphous alloys, Nanoperm, or Permalloy). This is mostly due to very low magnetostriction λ_s and relatively small M_s. As already highlighted, choosing an optimisation based on volume/weight or cost totally changes the definition of the most efficient material.

5. Conclusion

In this paper, the area of Ericsson cycles under uniaxial magneto-elastic loading was used as an indicator of energy harvesting capabilities of various magnetic materials. An analytical model was developed. The model is based on standard material parameters (saturation

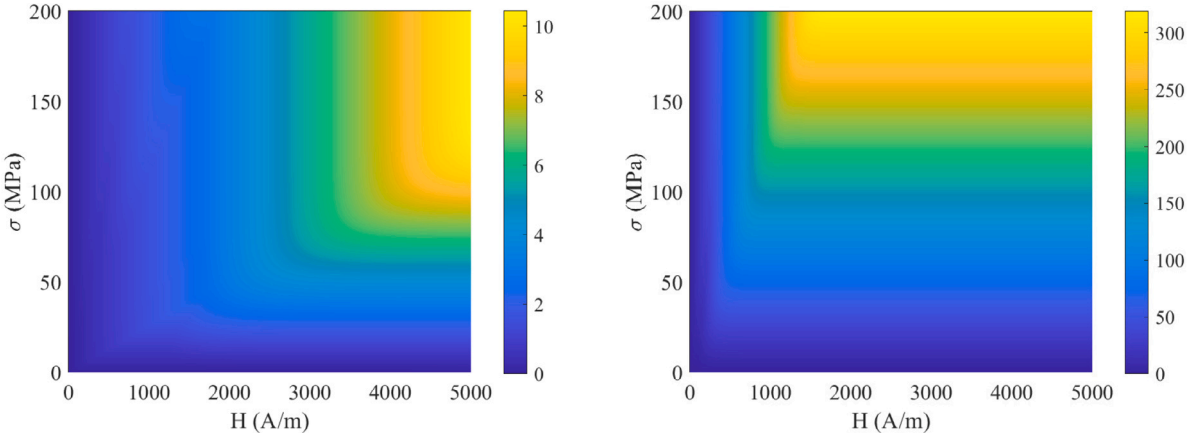

(a) Energy per volume unit (mJ.cm^{-3}) (b) Energy per price unit (mJ.\$$^{-1}$)

Fig. 2. Maximum harvestable energy for all tested materials as a function of the loading conditions (uniaxial configuration with compressive stress).

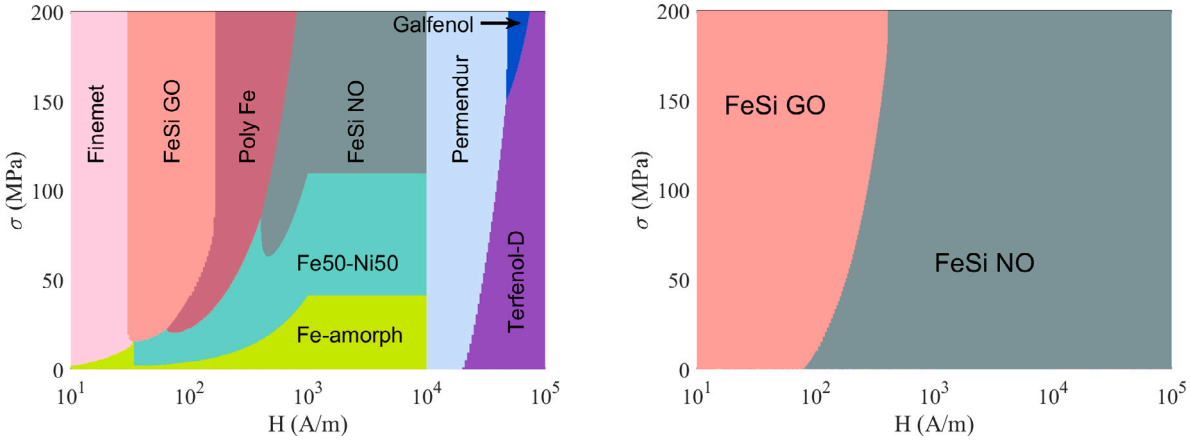

(a) Material performance map: volume efficiency (b) Material performance map: price efficiency

Fig. 3. Material performance maps: most efficient material depending on the loading conditions (uniaxial configuration with compressive stress). Magnetic field amplitude is shown in log scale.

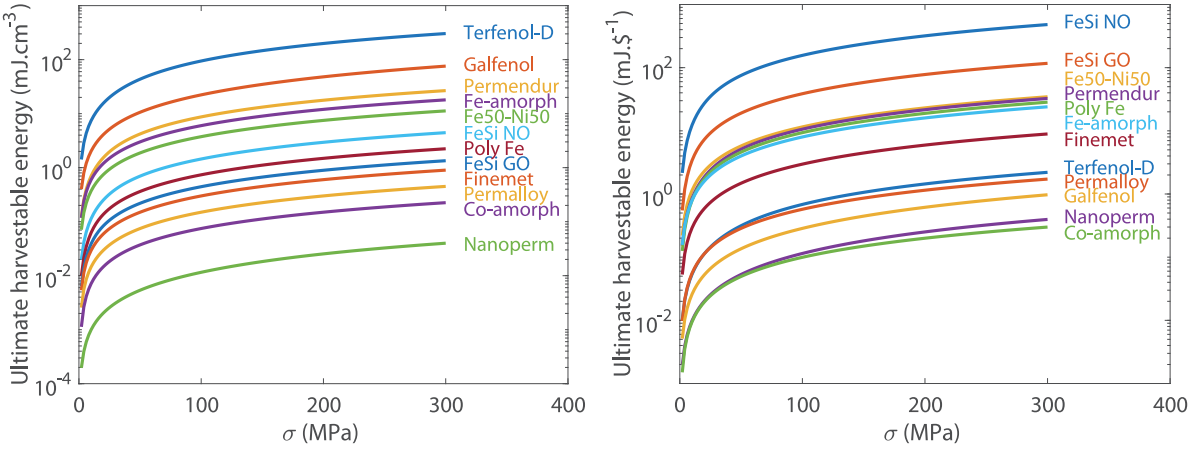

(a) Energy per volume unit (mJ.cm^{-3}) (b) Energy per price unit (mJ.\$$^{-1}$)

Fig. 4. Ultimate harvestable energy for all tested materials as a function of the available stress amplitude (uniaxial configuration).

magnetisation M_s, maximum magnetostriction λ_s, initial anhysteretic susceptibility of the stress-free magnetisation curve χ^o, coercive field H_c, mass density ρ and price $p_\$$). For configurations when a bias field H_b is used for energy harvesting the coercive field H_c can be replaced by H_b in the obtained formulas. The approach is based on an anhysteretic formulation of the magnetisation curves. Hysteresis is simply obtained by shifting the anhysteretic curve by a constant magnetic field value. A possible improvement would consist in incorporating

hysteresis effects in a more refined way. However, it is believed that the proposed formula allows to capture the main trends of the evolution of the Ericsson cycles under different magneto-elastic configurations.

The model was used to compare various materials with respect to their energy harvesting potential. The comparison was performed for the case of uniaxial magneto-elastic loadings but the model is applicable to multiaxial configurations. It is shown that when optimising volume (or weight) Giant Magnetostrictive materials (Terfenol-D and Galfenol) offer the highest efficiency for energy harvesting if no limitation is given on the amplitude of the magnetic field. However if high values of magnetic field cannot be reached, some iron-based materials appear as challengers. Below magnetic field levels of a few thousands A m^{-1}, Giant Magnetostrictive Materials are no longer competitive. Based on price, the game is totally changed and electrical steels appear to be excellent candidates for energy harvesting applications. Of course, prices are subject to considerable variations depending on availability, required volume, supplier or time, so that the conclusions drawn can be rapidly outdated. Similarly, material properties can evolve significantly depending on compositions or processes. But the analytical criterion proposed allows easy and continuous updating. It is also worth noting that the material is not everything in the design of an energy harvesting device, and the volume and cost of the surrounding system also plays a role, which was not discussed in this study.

CRediT authorship contribution statement

Laurent Daniel: Conceptualization, Methodology, Software, Investigation, Visualization, Writing – original draft. **Benjamin Ducharne:** Conceptualization, Investigation, Resources, Writing – review & editing. **Yuanyuan Liu:** Validation, Writing – review & editing. **Gael Sebald:** Conceptualization, Validation, Writing – review & editing.

Declaration of competing interest

The authors declare that they have no known competing financial interests or personal relationships that could have appeared to influence the work reported in this paper.

Data availability

No data was used for the research described in the article.

Appendix. Applicability of energy harvesting devices based on Ericsson cycles

This article compares the harvesting capability of different magnetostrictive materials based on the Ericsson cycle. In order to support the significance of this theoretical approach, we show in this appendix how the Ericsson cycle can be used as an actual energy harvesting cycle. The objective is notably to show that the harvested energy can significantly exceed the amount required for the cycle creation.

The generation of a real-timely controlled, high-amplitude magnetic excitation is a critical aspect. Permanent magnets used in electromagnetic devices generate magnetic fields of constant amplitude, which is unsuitable in the Ericsson cycle context. Excitation coils are the only alternative option, but to the price of Joule losses. These losses constitute a large proportion of the total input energy required by the cycle generation. Therefore, a good approximation of the real amount of energy harvested can be obtained from the ratio r between the amount of harvested energy W_{harv} and the amount of energy W_{J} lost by Joule effect in the excitation coil:

$$r = \frac{W_{\mathrm{harv}}}{W_{\mathrm{J}}} \tag{A.1}$$

Based on such analysis, optimised experimental conditions can be given to maximise the ratio r, inspired from the study case in [16].

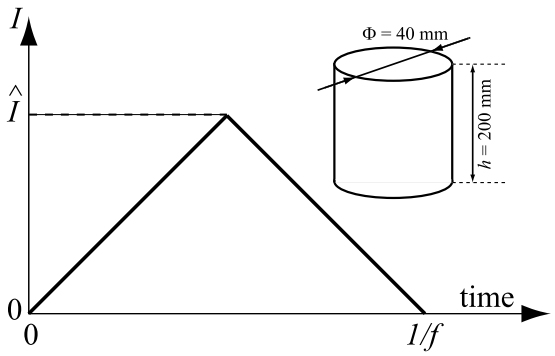

Fig. A.5. Rod specimen and electrical current waveform.

Consider a rod of magnetostrictive material, with diameter $\Phi = 40$ mm and height $h = 200$ mm (Fig. A.5). The excitation field H_m is tested in the range [0.1 100] kA m^{-1}, and the maximal current I is imposed to be no larger than 10 A. The coil wire diameter Φ_{w} is set to ensure a temperature elevation $\Delta\theta$ lower than 50 °C. A first calculus based on (A.2) is done to estimate the height h_{c} of the resulting coil, where N is the number of turns, n_{lay} the number of layers for the coil, and $\rho_{\mathrm{corr}} = 1.1$ a correction coefficient to take into account the wire dielectric coating and some potential irregularities in the turns distribution.

$$h_{\mathrm{c}} = \rho_{\mathrm{corr}} \frac{N \Phi_{\mathrm{w}}}{n_{\mathrm{lay}}} \tag{A.2}$$

Several conclusions can be drawn from the exploitation of (A.2) in the physical and geometrical conditions described above ($H_m \in$ [0.1 100] kA m^{-1}, $I \leq 10$ A, $\Delta\theta \leq 50$ °C). For this, h_{c} was calculated for every possible combination of working conditions and considering up to 5 layers (n_{lay}):

- n_{lay} has to be larger than 25 to generate $H_m = 100$ kA m^{-1} while keeping h_{c} lower than h.
- a single layer coil is enough to generate up to $H_m = 1$ kA m^{-1}
- three layers are the minimal requirement to reach $H_m = 10$ kA m^{-1}

The Joule losses can then be calculated using (A.3), where R is the in-series coil resistance, and f is the frequency of current waveform, assumed triangular (Fig. A.5).

$$W_{\mathrm{J}} = \frac{R I^2}{3f} \tag{A.3}$$

On the other hand, W_{harv} is obtained by multiplying the results from Table 2 by the volume of the considered magnetostrictive materials (aprox. 250 cm^3 with the geometry considered here). The calculation of r is limited here to the materials identified in the study as potential candidates for energy harvesting applications:

- FeSi NO and FeSi GO from Table 3 criterion
- Fe-amorph from Table 2 criterion at low magnetic fields
- Terfenol-D from Table 2 criterion at high magnetic fields

The ratio r is presented for the selected materials in Table A.4. The practically of use of an Ericsson cycle is set - arbitrarily - for ratios r above 5 (green-coloured cells in Table A.4). In the low field range ($H_m = 100$ A m^{-1}), this criterion is met for all materials. Oppositely, only Terfenol-D fulfils this criterion in the high field range. FeSi GO exhibits the largest r (>60) but only in the low field range where the amount of harvested energy is limited. Of course these results are dependent on the specimen geometry, but provide the trends for material performance.

Finally, to assess the practicality of energy harvesting from Ericsson cycles, the question of the electrical converter has to be considered. A possibility is to consider a bidirectional DC–DC converter. Based the energy densities reported in Table 2 and with the considered geometry, electrical powers in the range of [1 250] W at $f = 50$ Hz are expected.

Table A.4
Ratio r for different current I and stress σ levels for a selection of magnetostrictive materials. A light colour indicates a ratio $r > 5$ and a dark colour indicates $r > 25$. Uniaxial stress is compressive ($\sigma < 0$).

	I (A)	1	5	10	1	5	10	1	5	10	1	5	10
	H_m (kA m^{-1})	0.1	0.1	0.1	1	1	1	10	10	10	100	100	100
	N	20	4	2	200	40	20	2000	400	200	20 000	4000	2000
10 MPa	FeSi NO	11.00	10.96	10.92	4.04	4.03	4.01	0.40	0.40	0.40	0.04	0.04	0.04
10 MPa	FeSi GO	13.83	13.79	13.73	1.38	1.38	1.37	0.14	0.14	0.14	0.01	0.01	0.01
10 MPa	Fe-amorph	51.08	50.93	50.70	21.18	21.11	21.02	2.12	2.11	2.10	0.21	0.21	0.21
10 MPa	Terfenol-D	3.55	3.54	3.52	0.28	0.28	0.28	0.50	0.50	0.50	2.23	2.23	2.22
25 MPa	FeSi NO	18.44	18.39	18.31	1.84	1.84	1.83	0.18	0.18	0.18	0.02	0.02	0.02
25 MPa	FeSi GO	37.60	37.49	37.32	3.76	3.75	3.73	0.38	0.37	0.37	0.04	0.04	0.04
25 MPa	Fe-amorph	51.08	50.93	50.70	5.11	5.09	5.07	0.51	0.51	0.51	0.05	0.05	0.05
25 MPa	Terfenol-D	7.45	7.43	7.39	0.74	0.74	0.74	0.07	0.07	0.07	0.01	0.01	0.01
50 MPa	FeSi NO	19.86	19.81	19.72	24.69	24.62	24.51	2.47	2.46	2.45	0.25	0.25	0.25
50 MPa	FeSi GO	62.43	62.25	61.97	7.77	7.75	7.71	0.78	0.77	0.77	0.08	0.08	0.08
50 MPa	Fe-amorph	51.08	50.93	50.70	53.20	53.05	52.81	10.64	10.61	10.56	1.06	1.06	1.06
50 MPa	Terfenol-D	11.00	10.96	10.92	0.92	0.92	0.92	1.67	1.67	1.67	11.35	11.32	11.27
100 MPa	FeSi NO	19.86	19.81	19.72	51.18	51.04	50.81	4.97	4.95	4.93	0.50	0.50	0.49
100 MPa	FeSi GO	62.78	62.60	62.32	15.75	15.70	15.63	1.57	1.57	1.56	0.16	0.16	0.16
100 MPa	Fe-amorph	51.08	50.93	50.70	53.20	53.05	52.81	5.32	5.31	5.28	0.53	0.53	0.53
100 MPa	Terfenol-D	13.48	13.44	13.38	1.14	1.13	1.13	2.03	2.02	2.01	17.73	17.68	17.60

For such powers, commercially available DC–DC converters such as MAX797 [38] or MAX1653 [39] exhibit up to 96% efficiency. A rough estimation can be obtained for the voltage amplitude based on (A.4), where S is the rod cross-section, ω the angular velocity, and ΔB the maximal variation of the magnetic induction along with the Ericsson cycle.

$$V = n\,S\,\omega\,\Delta B \tag{A.4}$$

A few volts are obtained in the low field range and up to more than 1000 V in the extreme case of the Terfenol-D for $H_m = 100$ kA m^{-1} and $N = 20\,000$ turns. Besides this extreme case, all coloured cells in Table A.4 lead to reasonable values, low enough to be used as input of the proposed DC–DC converters.

References

[1] N. Panayanthatta, G. Clementi, M. Ouhabaz, M. Costanza, S. Margueron, A. Bartasyte, S. Basrour, E. Bano, L. Montes, C. Dehollain, R. La Rosa, A self-powered and battery-free vibrational energy to time converter for wireless vibration monitoring, Sensors 21 (22) (2021) 7503.

[2] S. Zeadally, F.K. Shaikh, A. Talpur, Q.Z. Sheng, Design architectures for energy harvesting in the internet of things, Renew. Sustain. Energy Rev. 128 (2020) 109901.

[3] P. Kamalinejad, C. Mahapatra, Z. Sheng, S. Mirabbasi, V.C. Leung, Y.L. Guan, Wireless energy harvesting for the internet of things, IEEE Commun. Mag. 53 (6) (2015) 102–108.

[4] K. Veni Selvan, M.S.M. Ali, Micro-scale energy harvesting devices: Review of methodological, Renew. Sustain. Energy Rev. 54 (2016) 1035–1047.

[5] J. Krikke, Sunrise for energy harvesting products, IEEE Pervasive Comput. 4 (1) (2005) 4–5.

[6] Z. Deng, M.J. Dapino, Review of magnetostrictive vibration energy harvesters, Smart Mater. Struct. 26 (10) (2017) 103001.

[7] G. Backman, B. Lawton, N.A. Morley, Magnetostrictive energy harvesting: Materials and design study, IEEE Trans. Magn. 55 (7) (2019) 1–6.

[8] J. Hu, F. Xu, A.Q. Huang, F.G. Yuan, Optimal design of a vibration-based energy harvester using magnetostrictive material (MsM), Smart Mater. Struct. 20 (1) (2010) 015021.

[9] A. Viola, V. Franzitta, G. Cipriani, V. Di Dio, F.M. Raimondi, M. Trapanese, A magnetostrictive electric power generator for energy harvesting from traffic: Design and experimental verification, IEEE Trans. Magn. 51 (11) (2015) 1–4.

[10] S.P. Beeby, T. O'Donnell, Electromagnetic energy harvesting, in: S. Priya, D.J. Inman (Eds.), Energy Harvesting Technologies, Springer, Boston, 2009.

[11] F.U. Khan, M.U. Qadir, State-of-the-art in vibration-based electrostatic energy harvesting, J. Micromech. Microeng. 26 (10) (2016) 103001.

[12] H. Liu, J. Zhong, C. Lee, S.W. Lee, L. Lin, A comprehensive review on piezoelectric energy harvesting technology: Materials, mechanisms, and applications, Appl. Phys. Rev. 5 (4) (2018) 041306.

[13] F. Narita, M. Fox, A review on piezoelectric, magnetostrictive, and magnetoelectric materials and device technologies for energy harvesting applications, Adv. Eng. Mater. 20 (2018) 1700743.

[14] T. Ueno, Magnetostrictive vibrational power generator for battery-free IoT application, AIP Adv. 9 (3) (2019) 035018.

[15] X. Zhao, D.G. Lord, Application of the Villari effect to electric power harvesting, J. Appl. Phys. 99 (8) (2006) 08M703.

[16] M. Zucca, M. Hadadian, O. Bottauscio, Quantities affecting the behavior of vibrational magnetostrictive transducers, IEEE Trans. Magn. 51 (1) (2015) 8000104.

[17] B. Yan, C. Zhang, L. Li, Magnetostrictive energy generator for harvesting the rotation of human knee joint, AIP Adv. 8 (5) (2018) 056730.

[18] R. Mech, P. Wiewiórski, K. Wachtarczyk, Use of magnetomechanical effect for energy harvesting and data transfer, Sensors 22 (9) (2022) 3304.

[19] T. Ueno, S. Yamada, Performance of energy harvester using iron–gallium alloy in free vibration, IEEE Trans. Magn. 47 (10) (2011) 2407.

[20] V. Berbyuk, Vibration energy harvesting using galfenol-based transducer, in: Active and Passive Smart Structures and Integrated Systems 2013, Vol. 8688, SPIE, 2013, p. 429.

[21] S. Palumbo, P. Rasilo, M. Zucca, Experimental investigation on a Fe-Ga close yoke vibrational harvester by matching magnetic and mechanical biases, J. Magn. Magn. Mater. 469 (2019) 354.

[22] C. Clemente, D. Davino, Modeling and characterization of a kinetic energy harvesting device based on galfenol, Materials 12 (19) (2019) 3199.

[23] L. Wang, C. Lian, D. Shu, Z. Yan, X. Nie, Analytical solution and optimal design for the output performance of galfenol cantilever energy harvester considering electromechanical coupling effect, Sci. Rep. 13 (2023) 12857.

[24] L. Wang, F.G. Yuan, Vibration energy harvesting by magnetostrictive material, Smart Mater. Struct. 17 (4) (2008) 045009.

[25] M. Zucca, O. Bottauscio, C. Beatrice, F. Fiorillo, Modeling amorphous ribbons in energy harvesting applications, IEEE Trans. Magn. 47 (10) (2011) 4421.

[26] H. Kurita, K. Katabira, Y. Yoshida, F. Narita, Footstep energy harvesting with the magnetostrictive fiber integrated shoes, Materials 12 (13) (2019) 2055.

[27] S.I. Yamaura, T. Nakajima, Y. Kamata, T. Sasaki, T. Sekiguchi, Production of vibration energy harvester with impact-sliding structure using magnetostrictive fe-co-v alloy rod, J. Magn. Magn. Mater. 514 (2020) 167260.

[28] A. Sisman, H. Saygin, On the power cycles working with ideal quantum gases: I. The ericsson cycle, J. Phys. D: Appl. Phys. 32 (6) (1999) 664.

[29] Y. Liu, B. Ducharne, G. Sebald, K. Makihara, M. Lallart, Investigation of energy harvesting capabilities of metglas 2605sa1, Appl. Sci. 13 (6) (2023) 3477.

[30] L. Daniel, An analytical model for the effect of multiaxial stress on the magnetic susceptibility of ferromagnetic materials, IEEE Trans. Magn. 49 (5) (2013) 2037–2040.

[31] L. Daniel, O. Hubert, M. Rekik, A simplified 3D constitutive law for magneto-mechanical behaviour, IEEE Trans. Magn. 51 (3) (2015) 7300704.

[32] L. Bernard, B.J. Mailhé, N. Sadowski, N.J. Batistela, L. Daniel, Multiscale approaches for magnetoelasticity in device simulation, J. Magn. Magn. Mater. 497 (2019) 165241.

[33] L. Daniel, L. Bernard, O. Hubert, Multiscale modelling of magnetic materials, in: Abdul-Ghani Olabi (Ed.), Encyclopedia of Smart Materials, Vol. 5, Oxford : Elsevier, 2022, pp. 32–49, http://dx.doi.org/10.1016/B978-0-12-803581-8.12056-9.

[34] L. Daniel, M. Domenjoud, Anhysteretic magneto-elastic behaviour of terfenol-d: experiments, multiscale modelling and analytical formulas, Materials 14 (18) (2021) 5165.

[35] F. Fiorillo, Magnetic Materials for Electrical Applications: A Review, INRIM Technical Report 13/2010, 2010.

[36] M. Domenjoud, E. Berthelot, N. Galopin, R. Corcolle, Y. Bernard, L. Daniel, Characterization of giant magnetostrictive materials under static stress: influence of loading boundary conditions, Smart Mater. Struct. 28 (9) (2019) 095012.

[37] M. Domenjoud, A. Pécheux, L. Daniel, Characterization and multiscale modeling of the magneto-elastic behavior of galfenol, IEEE Trans. Magn. (2023) http://dx.doi.org/10.1109/TMAG.2023.3280925.

[38] Step-down controllers with synchronous rectifier for CPU power, MAX797, analog devices. [online]. available: https://www.analog.com/en/products/max797.html#product-overview.

[39] High-efficiency, PWM, step-down DC-DC controllers in 16-pin QSOP, MAX1653, analog devices. [online]. available: https://www.analog.com/en/products/max1653.html#product-overview.